Fabrication of Polymer Nanocavities with Tailored Openings

Li Huey Tan,[†] Shuangxi Xing,[†] Tao Chen,[†] Gang Chen,[†] Xiao Huang,[‡] Hua Zhang,[‡] and Hongyu Chen[†,*]

[†]Division of Chemistry and Biological Chemistry, Nanyang Technological University, 21 Nanyang Link, 637371 Singapore, and [‡]School of Materials Science and Engineering, Nanyang Technological University, 50 Nanyang Avenue, 639798 Singapore

ABSTRACT A templated fabrication of open nanocavities is reported, where rational control of partial polymer attachment on sacrificial metal cores introduces openings in the polymer shells. This approach provides a facile means to modify the structural features of polymer nanocavities by manipulating the surface chemistry of colloidal nanoparticles. In particular, the anisotropic geometry of gold nanorods is exploited to promote the anisotropic polymer attachment, such that two diametric openings occurred in the polymer shell. After etching the gold nanorods, this approach yields open nanochannels that are tunable in both diameter and length. The synthetic scope of the anisotropic core/shell nanoparticles is expanded, supporting the previously proposed mechanism. We demonstrate that reducing the symmetry of nano-objects could open up new ways to create structural features using simple assembly and etching techniques. The thermostability of the open polymer nanostructures is also investigated.

KEYWORDS: nanocavity · anisotropic encapsulation · etching · linear aggregation · self-assembly

Nanocavities have attracted great interest due to their potential applications as sensors, catalyst carriers, nanoreactors, and delivery vessels;[1−5] broader applications can be envisioned if hollow nanostructures could be prepared with tailored composition and morphology. The various nanocavities employed by Nature, such as lipid vesicles and gated ionic channels, clearly demonstrate the potentials of such controls.

Synthetic nanocavities have been realized only in a few systems. Vesicles and nanotubes were prepared by self-assembly of amphiphiles such as block copolymers[6] and lipid-like small molecules.[7−9] However, as a result of the self-assembly, these nanostructures are largely dictated by the chemical nature of the constituent amphiphiles and cannot be readily tailored. A second class of nanocavity was derived from core−shell nanoparticles (NPs), by sacrificing the core component.[10−14] The size and shape of the resulting cavities can be readily controlled by the choice of the initial core,[15,16] though the overall shells were generally isotropic and lacked openings. Such cavities are not ideal for applications such as channels or joints for nanodevices. Mesoscale (0.1−10 μm) hollow structures with openings were previously reported,[17−20] but few examples in the literature were of open nanocavities (<100 nm). Nanocages prepared by etching AgNPs with $HAuCl_4$ have multiple openings,[21] and nanotubes prepared by amphiphile self-assembly often have inherent open ends.[7,8] In general, however, introducing openings in the nanocavity has been a major challenge, and rational control of the size and position of the openings has yet to be realized.

Here, we report a templated fabrication of open polymer nanocavities that resulted from rational control of partial polymer attachment on sacrificial metal cores (Figure 1a). By etching these cores, openings appeared at positions initially not covered by the polymer. This strategy is an advancement of our previously reported synthesis of Janus (two-sided) NPs, whereby the competitive binding of hydrophobic (L_A, *e.g.*, 2-dipalmitoyl-*sn*-glycero-3-phosphothioethanol (sodium salt) (**2**); see Table 1) and hydrophilic ligands (L_B, *e.g.*, diethylamine (**5**)) on Au nanospheres (AuNSs) led to anisotropic attachment of amphiphilic diblock copolymer, polystyrene-*block*-poly(acrylic acid) (PS-*b*-PAA).[22] (In the following text, the abbreviation *aniso*-(**L_A**+**L_B**-NP)@PSPAA is used to represent such anisotropic core/shell nanostructures.) The synthetic scope was now expanded, including a variety of cores, polymers, and ligand combinations. This allowed

*Address correspondence to hongyuchen@ntu.edu.sg.

Received for review August 2, 2009 and accepted October 1, 2009.

Published online October 9, 2009.
10.1021/nn900917z CCC: $40.75

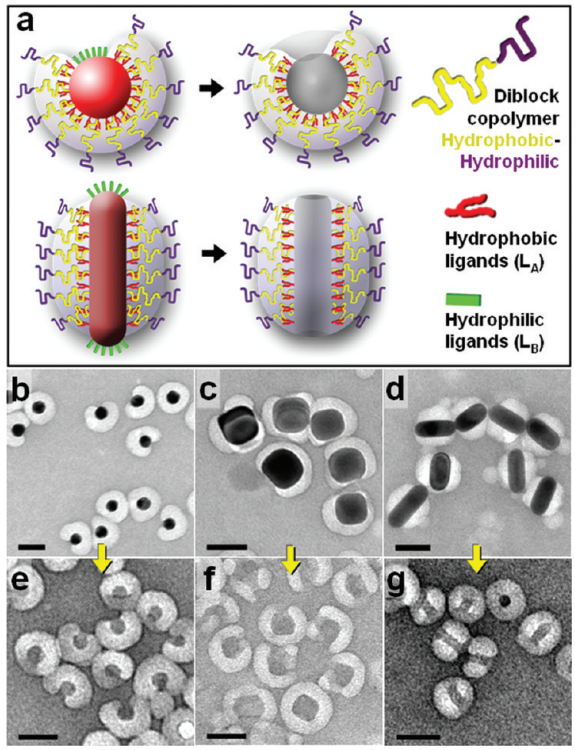

Figure 1. (a) Schematics for the anisotropically encapsulated AuNSs and AuNRs, and the formation of the respective nanocavities; (b−d) TEM images of anisotropically encapsulated AuNSs, AgNCs, and AuNRs, respectively; (e-g) corresponding polymer cavities after etching the metal cores in samples (b−d). Scale bars: 50 nm.

the structural features of the partial polymer shell to be tailored by modifying the surface chemistry of the metal cores. In particular, openings can be created and rationally controlled in polymer nanostructures, which are generally more stable than those generated by the self-assembly of small molecules.

RESULTS AND DISCUSSION

The anisotropic core/shell NPs were prepared by a one-step synthesis: a mixture of AuNSs, PS-*b*-PAA, L_A, and L_B in DMF/H_2O (4:1) was heated at 110 °C for 2 h and then slowly cooled to room temperature.[22] As the critical micelle concentration of PS-*b*-PAA decreased with temperature, the polymer became less soluble in solution and selectively assembled on L_A-covered regions of the AuNS. The polystyrene (PS) blocks formed a spheroidal shell to minimize the surface/volume ratio, while the soluble poly(acrylic acid) (PAA) blocks created a corona layer on the surface (Figure 1a), introducing charge and steric repulsion against aggregation. After the synthesis, the solution was diluted by water to extract DMF from the PS cores and trap the polymer micelles in kinetically stable states. The solution was then centrifuged to remove excess reactants and empty polymer micelles before the product was characterized by transmission electron microscopy (TEM). The competition between L_A and L_B determines the ligand coverage ratio on AuNSs,[22] which could be tuned by the choice of the ligands and their concentrations.

A variety of ligands were found to be compatible with this synthesis. L_A could be thiol-ended molecules with aliphatic chains (1-octadecanethiol (**1**) and **2**) or aromatic groups (2-naphthalenethiol (**3**) and 4-ethylthiophenol (**4**)), while L_B typically has polar (2-mercaptoacetic acid (**7**) and 4-mercaptobenzoic acid (**8**)) or short aliphatic groups (**5** and 1-ethanethiol (**6**)). A full list of the tested ligand combinations is given in Table 1 with references to the corresponding TEM images. The relative lengths of PS or PAA chains are not essential to the anisotropic encapsulation; PS_{154}-*b*-PAA_{60}, PS_{144}-*b*-PAA_{28}, and PS_{404}-*b*-PAA_{62} have all been shown to be viable (Table 1 and Figure 2). Moreover, several types of metal NPs were found to be compatible, including (a) the negatively charged, citrate-stabilized AuNSs,[22] (b) the positively charged, hexadecyltrimethylammonium bromide (CTAB)-stabilized Au nanorods (AuNRs, Figures 1d and 5a), and (c) the charge-neutral, polyvinylpyrrolidone (PVP)-stabilized

TABLE 1. Chemical Structures of the Tested Hydrophobic (L_A) and Hydrophilic Ligands (L_B) and the Known Conditions That Gave *aniso*-NP@PSPAA Using Different Combinations of Cores, Polymers, L_A, and L_B

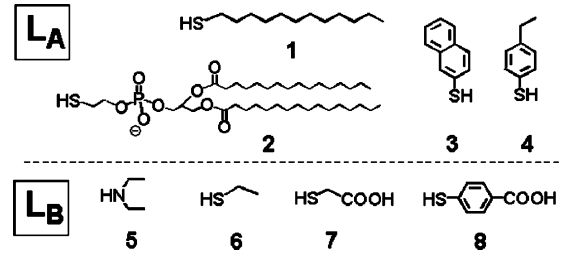

Core	Polymer	L_A	L_B	Reference	Verified Structures[a]
Au	$PS_{154}PAA_{60}$	2	5	Ref. 22	
Au	$PS_{154}PAA_{60}$	2	6	Figure 1b	
Au	$PS_{154}PAA_{60}$	2	8	Figure 2a	
Au	$PS_{154}PAA_{60}$	2	7	Figure 2b	
Au	$PS_{154}PAA_{60}$	1	7	Figure 2c	
Au	$PS_{154}PAA_{60}$	3	6	Figure 5c	
Au	$PS_{154}PAA_{60}$	3	6	Figure 2d	
Au	$PS_{154}PAA_{60}$	4	6	Figure 2e	
Au	$PS_{144}PAA_{28}$	2	6	Figure 2f	
Au	$PS_{144}PAA_{28}$	2	8	Figure 2g	
Au	$PS_{404}PAA_{62}$	2	6	Figure 2h	
Au	$PS_{144}PAA_{28}$	2	8	Figure 1d	
Au	$PS_{154}PAA_{60}$	2	8	Figure 2i	
Ag	$PS_{154}PAA_{60}$	2	6	Figure 1c	

[a]Structures reported here have been produced in experiments but may not reflect the complete scope attainable by varying the L_A/L_B ratio.

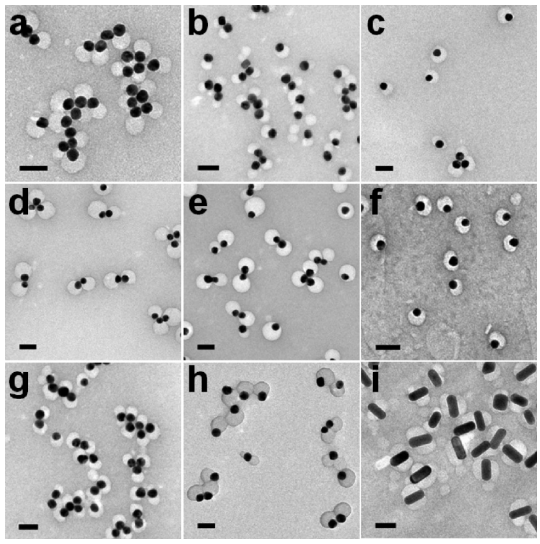

Figure 2. Typical TEM images of the (a) *aniso*-(2+8-AuNS)@$PS_{154}PAA_{60}$ ([8]/[2] = 1.37); (b) *aniso*-(2+7-AuNS)@$PS_{154}PAA_{60}$ ([7]/[2] = 0.27); (c) *aniso*-(1+7-AuNS)@$PS_{154}PAA_{60}$ ([7]/[1] = 5.0, 150 °C); (d) *aniso*-(3+6-AuNS)@$PS_{154}PAA_{60}$ ([6]/[3] = 7.41, 150 °C, 3 h); (e) *aniso*-(4+6-AuNS)@$PS_{154}PAA_{60}$ ([6]/[4] = 2.40, 130 °C, 6 h); (f) *aniso*-(2+6-AuNS)@$PS_{144}PAA_{28}$ ([6]/[2] = 1.27); (g) *aniso*-(2+8-AuNS)@$PS_{144}PAA_{28}$ ([8]/[2] = 1.37, V_{DMF}/V_{H_2O} = 3.5); (h) *aniso*-(2+6-AuNS)@$PS_{404}PAA_{62}$ ([6]/[2] = 3.17); and (i) *aniso*-(2+8-AuNR)@$PS_{154}PAA_{60}$ ([8]/[2] = 2.28). Conditions were V_{DMF}/V_{H_2O} = 3.5, heated at 110 °C for 2 h unless otherwise stated. Polymer attachment is less uniform for systems in (d) and (e) probably due to the unique packing of the ligands 3 and 4. Scale bars: 50 nm.

Ag nanocubes (AgNCs, Figure 1c). In the latter two cases, the excess capping ligands from the NP synthesis (CTAB and PVP) have to be removed before the encapsulation. This ensured the domination of NP surface by L_A and L_B, which dictate the polymer attachment.

A new type of Janus NPs was observed when **2** and **6** were used as ligands. At [**6**]/[**2**] = 1.27, the resulting *aniso*-(**2**+**6**-AuNS)@PSPAA were highly uniform and revealed only a slight opening of ~8 nm wide, about 1/50 of the total AuNS (d = 25.7 ± 1.9 nm) surface area (Figure 1b). Previously, the openings generated using ligands **2** and **5**, at its smallest, were ~1/3 of total Au surface area (at [**5**]/[**2**] = 22), where the spheroidal polymer micelles were roughly tangent to the AuNSs.[22] The etching of these anisotropic structures led to only unimpressive shallow nanopockets (Figure S1d in Supporting Information). Attempts to further reduce the openings by decreasing the [**5**]/[**2**] ratio, however, did not lead to continually smaller openings but instead gave fully encapsulated AuNSs (*e.g.*, at [**5**]/[**2**] = 1.27, Figure S5a in Supporting Information). At low concentrations, ligand **5** appeared to have been completely ousted by **2**. In comparison, a strong Au-binding ligand such as **6** allowed the retaining of an even small hydrophilic region in the *aniso*-(**2**+**6**-AuNS)@PSPAA. With the small openings in the polymer shells, the AuNSs appeared to sink deeper in the spheroidal micelles, creating a thick polymer wall at the openings. This unique structure led to deep nanopockets after removal of the Au core (Figure 1e).

The distinctive symmetry of AgNCs and AuNRs led to interesting development of partial polymer coverage on these NPs. The polymer openings on AgNCs were quite irregular, often occurring at one or several cube faces. In contrast, the *aniso*-(**2**+**8**-AuNR)@PSPAA were highly uniform, with two openings occurring on both ends of each AuNRs (Figure 1d). As far as we know, the specific encapsulation on the sides but not the ends of AuNRs has not been achieved using any kind of shell. In both cases, complete encapsulation ensued when L_B was not used (Figure S5b in Supporting Information),[23] thereby reaffirming the role of L_B ligands and its competition with L_A in the formation of the anisotropic polymer shells. The preferential attachment of polymer on the sides of AuNRs could be due to (a) the stronger affinity of L_B to the {111} facets at both ends,[24] (b) the less efficient packing of L_A at the high-curvature surface, or (c) the larger strain of polymer micelle at both ends. On the basis of the predominant appearance of openings on the {100} facets of AgNCs (Figure 1c,f), it appears that the ligand distribution was facet-specific, but evidently, this distribution was also influenced by polymer adsorption since not all {100} facets of AgNCs were exposed and the exposed area only consists of a small portion of the underlying facet.

Previously, the fully encapsulated *iso*-AuNS@PSPAA were shown to withstand CN^- etching for months, possibly because the ions cannot diffuse through the hydrophobic PS layer.[25,26] In contrast, the cores of *aniso*-AuNS@PSPAA readily dissolved when incubated in aqueous KCN (4 mM), as evident from the rapid disappearance of the surface plasmon absorption at 530 nm in ultraviolet−visible (UV−vis) spectra (Figure S7a in Supporting Information). The hydrophilic ligand layer obviously did not prevent the diffusion of both CN^- and $[Au(CN)_4]^-$. After etching, the polymer particles were purified by dialysis to remove excess reactants. The resulting hollow polymer particles can tolerate high-salt solutions (*e.g.*, 1 M NaCl at pH 10) similar to the *iso*-AuNS@PSPAA.[27] This extraordinary colloidal stability promises broad compatibility for future applications. While all of the *aniso*-AuNS@PSPAA characterized by TEM may not orient at the right perspectives to reveal the openings in the shell, few of them retained the AuNSs after the etching (Figure 1e). Statistics from 882 etched particles of *aniso*-(**2**+**6**-AuNS)@PSPAA indicated that 47% of them were hollow with observable openings, 48% were hollow without apparent openings, and only 4.9% still enclosed a AuNS. On the basis of these data, it can be estimated that the yield of the original *aniso*-AuNS@PSPAA was probably close to 95%. The nanopockets from *aniso*-(**2**+**6**-AuNS)@PSPAA (Figure 1e) have deeper cavities with smaller openings (width = 9.9 ± 2.4 nm) than those from *aniso*-(**2**+**5**-AuNS)@PSPAA (Figure S1d in Supporting Information). The

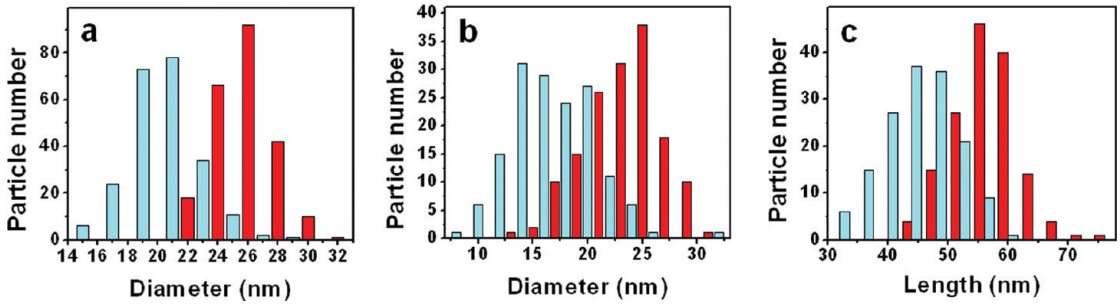

Figure 3. (a) Distribution of the diameter of (red) the *aniso*-(2+6-AuNS)@PSPAA core and (blue) the hollow cavity after etching. Distribution of (b) diameter and (c) length of (red) *aniso*-(2+8-AuNR)@PSPAA core and (blue) the hollow tube after etching.

overall hollow polymer structure was found to retain the shape of the template (d_{AuNS} = 25.7 nm), despite a slight shrinking of the cavity (d = 20.4 ± 2.2 nm) (Figure 3a). The openings became slightly larger after the etching, increasing from 8 to 9.9 nm. The structural integrity of the PS layer after removal of the internal support is most obvious in the case of *aniso*-(**2**+**6**-AgNC)@PSPAA, whereby the resulting cavity generally maintained the cubic shape (Figure 1f).

This is likely a result of the glassy nature of PS in the absence of organic solvent.[28] Unlike the micelles assembled from small molecules, the PS-*b*-PAA micelles are obviously resistant to the dissociation/reformation dynamics which would otherwise have eliminated the structural memory. Nevertheless, the polymer became more liquid-like at elevated temperature. The hollow polymer nanocavities were still intact when incubated at 60 °C in water for 2 h (Figure S5c in Supporting Information), but at 90 °C, the hollow structures collapsed (Figure 4a). The morphological transition occurred at a temperature close to the glass transition temperature of bulk polystyrene (100 °C).[29] To distinguish the collapsed polymer particles from the empty micelles of PS-*b*-PAA self-assembly, partially etched *aniso*-AuNS@PSPAA were induced to collapse. The remaining Au residues were found completely encapsulated, and no free AuNS was observed (Figure 4b). This clearly demonstrated that these micelles were not from PS-*b*-PAA

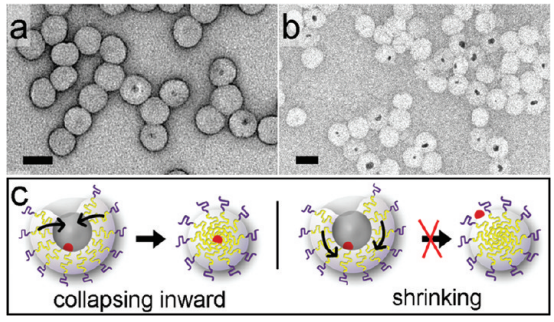

Figure 4. TEM images of (a) hollow NPs as shown in Figure 1e after fusing by heating at 90 °C, and (b) partially etched *aniso*-AuNS@PSPAA sample after heating at 100 °C. (c) Schematics of possible mechanisms, through which the hollow polymer particles could fuse by either collapsing inward (left) or shrinking of the PS core (right). Scale bars: 50 nm.

reassembly. Moreover, it suggests that the hollow polymer structure collapsed inward instead of withdrawing like a liquid which would have turned the Au residues outward (Figure 4c).

These results are unambiguous demonstration of the structural stability of the PS-*b*-PAA micelles. The size and morphology of the sacrificial cores and of the resulting cavities served as excellent markers for the structural degeneration under various conditions. The uniformity in the core sizes and shell structures allowed the collective behavior of the PS-*b*-PAA micelles to be conveniently studied, and the exceptional stability of the micelles in aqueous solution allowed the morphological transitions to be monitored directly by TEM images.

Unlike the spheroidal nanopockets templated by AuNSs or AgNCs, hollow polymer nanochannels (d = 16.9 ± 3.7 nm, l = 44.8 ± 5.9 nm, Figure 1g) were fabricated by removing Au from the *aniso*-(**2**+**8**-AuNR)@PSPAA. They are somewhat smaller than the original AuNRs (aspect ratio 2.4; d = 23.1 ± 3.4 nm, l = 56.7 ± 5.5 nm, Figure 3b,c). Importantly, the channels have two openings that resulted from the absence of polymer coverage at the ends of AuNRs. Structural control of these open nanochannels is facile in that the dimensions of the channels could be easily tuned by the choice of the template. AuNRs with high aspect ratio (18.0; d = 19 nm, l = 387 nm) were successfully encapsulated and subsequently etched to give long nanochannels with openings at both ends (Figure 5a,d, d = 18 nm, l = 367 nm). Compared to the open nanochannels prepared by amphiphile self-assembly,[7,8] the ones prepared by this templated approach are more versatile and more robust. To our knowledge, open nanochannels with monodispersed length have not been prepared previously.

The unique symmetry of *aniso*-AuNR@PSPAA provided an opportunity to linearly assemble them. As the L_B-coated surface is unstable in salt solution and the polymer is highly stable, incubation of these NRs in basic NaCl solution led to highly specific end-to-end aggregation (Figure 5b). After cross-linking the polymer shells to secure the organization, the Au cores were etched to give segmented nanochannels (Figure 5e). A

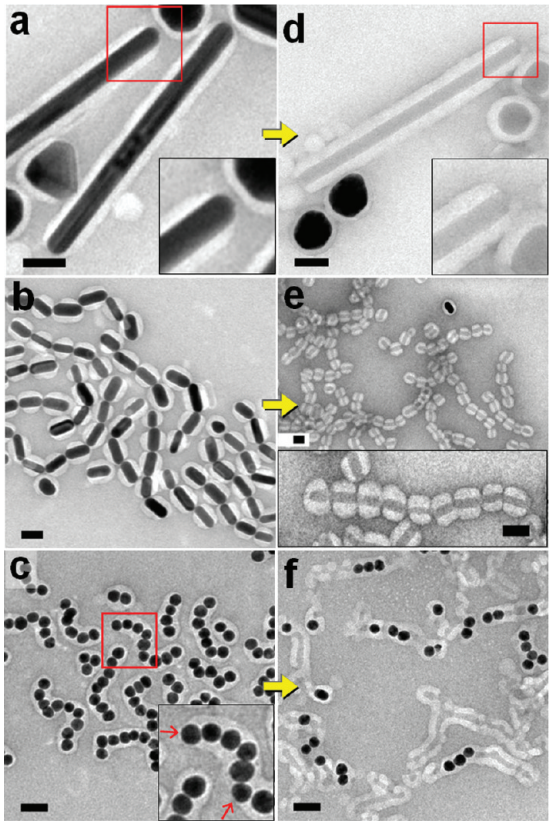

Figure 5. TEM images of (a) *aniso*-AuNR@PSPAA with aspect ratio 18; (b) linearly assembled *aniso*-AuNR@PSPAA (aspect ratio 2.4); (c) anisotropically encapsulated AuNS chains; and (d−f) corresponding polymer cavities after etching samples (a−c). Scale bars: 50 nm.

small percentage of the *aniso*-(**2**+**8**-AuNR)@PSPAA had only one opening, which limited the growth of the linear chains. On the basis of the survey of 914 polymer particles, it was found that 87.5% of the original *aniso*-(**2**+**8**-AuNR)@PSPAA had two openings, 11.1% had one opening, and 1.4% had no opening. It is conceivable that, with further improvement of the synthesis, this approach could lead to long, flexible nanochannels that could be functionalized along the length.

The anisotropic encapsulation was also applied to linear aggregates of AuNSs prepared by salt-induced aggregation (see Supporting Information). Openings in the polymer shells were found often at the ends and turning points of the AuNS chains (Figure 5c), which became obvious after the etching (Figure 5f). Since at these positions the AuNSs would unlikely have specific facets for the binding of L_B or specific packing for L_A, it is most likely that the strain of polymer micelles at high-curvature points is the dominant factor in determining polymer distribution. This observation argues against the selective L_A/L_B coordination on NPs as a sole determining factor for polymer coverage in *aniso*-NP@PSPAA.

SUMMARY

In summary, we have demonstrated a new method to introduce openings in polymer nanocavities, where the templated approach provided facile and precise controls of the polymer nanostructure. The size and shape of the cavity could be tailored by the choice of the sacrificial nanoparticles; the size of the openings could be manipulated by ligand competition during the anisotropic encapsulation; and the openings selectively occurred at both ends of gold nanorods. This approach is advantageous considering the scalable colloidal synthesis, the broad synthetic scope, and the stability of the resulting polymer nanostructures. As sophisticated nanodevices in the future will not be solely based on isotropic nanoparticles, breaking the symmetry of nanoparticles, as demonstrated in this report, will open up new ways to assemble nano-objects and to create new structural features for rational functional designs.

METHODS

AuNSs,[30] AuNRs with low[31] and high aspect ratio,[32] and AgNCs[33] were prepared based on the literature reports. The anisotropic encapsulation of NPs (a general name for AuNSs, AuNRs, and AgNCs), as listed in Table 1, was carried out according to the procedures of our previous paper[22] with modifications (more details available in Supporting Information).

Anisotropic Encapsulation of AuNRs (Aspect Ratio 2.4 ± 0.1; *d* = 23 nm, *l* = 57 nm): The as-synthesized, CTAB-stabilized AuNRs (1.5 mL) were concentrated by centrifugation to a volume of ~15 μL using 8100*g* for 10 min. The concentrated solution was then diluted with water to 1.5 mL and centrifuged to ~15 μL again to further remove the excess CTAB. The deep green solution collected was then diluted by water to a volume of 235 μL and then added to 750 μL of DMF solution, which was prepared by mixing PS_{144}-*b*-PAA_{28} (80 μL, 8 mg/mL in DMF), **8** (20 μL, 2 mM in EtOH), and DMF (670 μL). Ligand **2** (40 μL, 2 mg/mL in EtOH) was then finally added to the reaction mixture. The total volume of the final mixture was 1 mL, where V_{DMF}/V_{H_2O} = 3, [PS_{144}-*b*-PAA_{28}] = 0.039 mM, [**2**] = 0.22 mM, [**8**] = 0.04 mM. The mixture was heated at 110 °C for 2 h and then allowed to cool down gradually until room temperature. Similar procedures were used for the anisotropic encapsulation of high aspect ratio AuNRs and AgNCs; see Supporting Information for more details. Typically, when PS_{144}-*b*-PAA_{28} was used, the V_{DMF}/V_{H_2O} = 3, while V_{DMF}/V_{H_2O} = 4.5 and 8 were used for PS_{154}-*b*-PAA_{60} and PS_{404}-*b*-PAA_{62}, respectively. This is due to the different solubility of the polymers related to the different PS length and PS/PAA ratio.

Linear Aggregation of Anisotropically Encapsulated AuNRs: One hundred microliters of the as-synthesized *aniso*-(**2**+**8**-AuNR)@PSPAA was purified by centrifugation to ~10 μL. To induce aggregation, NaOH (l μL, 5 M) and NaCl (40 μL, 5 M) were added to this solution and the mixture was incubated overnight. The mixture were then diluted with 1.5 mL water and centrifuged at 8100*g* to remove the excess salt. Cross-linking of polymer shell for the linearly assembled *aniso*-(**2**+**8**-AuNR)@PSPAA was carried out by adding 1-ethyl-3-(3-dimethylaminopropyl) carbodiimide hydrochloride (EDC) (50 μL, 5.22 mM) to the purified sample (100 μL). The mixture was placed on a shaker for 30 min after which 2,2′-(ethylenedioxy)bis(ethylamine) (21.36 μL, neat), the cross-linker, was added to the mixture. The sample was left to react further for 30 min. After the completion of the reaction, the mixture was diluted with water to 1.5 mL and centrifuged at 8100*g* for 10 min to remove the excess reactants.

Etching by KCN: Regardless of the morphology, the *aniso*-NP@PSPAA sample (100 μL) was purified and concentrated to

10 μL. Then KCN (1 μL, 40 mM) was added to this concentrated sample. (CAUTION: KCN is extremely poisonous even at low concentrations; it should be handled with great care. Never add any acid to KCN solutions.) This mixture was left to react overnight, or until the original color of the sample disappears. This duration may vary from sample to sample. An aliquot (3 μL) of the sample was diluted with 8 μL of negative stain for TEM analysis without any purification. If the samples were used for further analysis, the sample was then dialyzed against water using Spectra/Por Dialysis Membrane (molecular weight cutoff = 25 000 Da) for 24 h. The residue supernatants and solutions were treated with excess $FeCl_3$ to detoxify the CN^- ions by forming $[Fe(CN)_6]^{3-}$.

Characterizations: JEM 1400 transmission electron microscope (JEOL) operated at 120 kV was used to obtain TEM images of the samples. $(NH_4)_6Mo_7O_{24}$ (3.4 mM) was used as the negative stain to improve contrast for all TEM images reported in this study. UV−vis spectra were collected on a Cary100 UV−vis spectrophotometer. Centrifugation was conducted on a brushless microcentrifuge Denville 260D angle rotor with centrifuging radius of 7.3 cm. Conversion to relative centrifugal force (RCF) was calculated with the formula RCF = $1.118 \times 10^{-5} \times 7.3$ (radius) $\times$ (speed in rpm)^2.

Acknowledgment. The authors thank financial supports from Ministry of Education, Singapore (RG 52/07 and ARC 27/07).

Supporting Information Available: Experimental procedures, large area view TEM images, and UV−vis spectra. This material is available free of charge *via* the Internet at http://pubs.acs.org.

REFERENCES AND NOTES

1. Geest, B. G. D.; Sanders, N. N.; Sukhorukov, G. B.; Demeester, J.; Smedt, S. C. D. Release Mechanisms for Polyelectrolyte Capsules. *Chem. Soc. Rev.* **2007**, *36*, 636–649.
2. Shchukin, D. G.; Sukhorukov, G. B. Nanoparticle Synthesis in Engineered Organic Nanoscale Reactors. *Adv. Mater.* **2004**, *16*, 671–682.
3. Peer, D.; Karp, J. M.; Hong, S.; Farokhzad, O. C.; Margalit, R.; Langer, R. Nanocarriers as an Emerging Platform for Cancer Therapy. *Nat. Nano* **2007**, *2*, 751–760.
4. Mann, S. Life as a Nanoscale Phenomenon. *Angew. Chem., Int. Ed.* **2008**, *47*, 5306–5320.
5. Christensen, S. M.; Stamou, D. Surface-Based Lipid Vesicle Reactor Systems: Fabrication and Applications. *Soft Matter* **2007**, *3*, 828–836.
6. Discher, D. E.; Eisenberg, A. Polymer Vesicles. *Science* **2002**, *297*, 967–973.
7. Zhou, Y.; Shimizu, T. Lipid Nanotubes: A Unique Template To Create Diverse One-Dimensional Nanostructures. *Chem. Mater.* **2008**, *20*, 625–633.
8. Shimizu, T.; Masuda, M.; Minamikawa, H. Supramolecular Nanotube Architectures Based on Amphiphilic Molecules. *Chem. Rev.* **2005**, *105*, 1401–1443.
9. Zhao, H.; Chen, J.-F.; Zhao, Y.; Jiang, L.; Sun, J.-W.; Yun, J. Hierarchical Assembly of Multilayered Hollow Microspheres from an Amphiphilic Pharmaceutical Molecule of Azithromycin. *Adv. Mater.* **2008**, *20*, 3682–3686.
10. Daniel, M.-C.; Astruc, D. Gold Nanoparticles: Assembly, Supramolecular Chemistry, Quantum-Size-Related Properties, and Applications toward Biology, Catalysis, and Nanotechnology. *Chem. Rev.* **2004**, *104*, 293–346.
11. Fan, H. J.; Gösele, U.; Zacharias, M. Formation of Nanotubes and Hollow Nanoparticles Based on Kirkendall and Diffusion Processes: A Review. *Small* **2007**, *3*, 1660–1671.
12. Caruso, F.; Caruso, R. A.; Mohwald, H. Nanoengineering of Inorganic and Hybrid Hollow Spheres by Colloidal Templating. *Science* **1998**, *282*, 1111–1114.
13. Xing, S.; Tan, L. H.; Yang, M.; Pan, M.; Lv, Y.; Tang, Q.; Yang, Y.; Chen, H. Highly Controlled Core/Shell Structures: Tunable Conductive Polymer Shells on Gold Nanoparticles and Nanochains. *J. Mater. Chem.* **2009**, *19*, 3286–3291.
14. Xing, S.; Tan, L. H.; Chen, T.; Yang, Y.; Chen, H. Facile Fabrication of Triple-Layer (Au@Ag)@Polypyrrole Core−Shell and (Au@H_2O)@Polypyrrole Yolk−Shell Nanostructures. *Chem. Commun.* **2009**, 1653–1654.
15. Cheng, D. M.; Xia, H. B.; Chan, H. S. O. Fabrication of Polymeric Hollow Nanospheres, Hollow Nanocubes and Hollow Plates. *Nanotechnology* **2006**, *17*, 1661–1667.
16. Obare, S. O.; Jana, N. R.; Murphy, C. J. Preparation of Polystyrene- and Silica-Coated Gold Nanorods and Their Use as Templates for the Synthesis of Hollow Nanotubes. *Nano Lett.* **2001**, *1*, 601–603.
17. Ma, G. H.; Su, Z. G.; Omi, S.; Sundberg, D.; Stubbs, J. Microencapsulation of Oil with Poly(styrene-*N*,*N*-dimethylaminoethyl methacrylate) by SPG Emulsification Technique: Effects of Conversion and Composition of Oil Phase. *J. Colloid Interface Sci.* **2003**, *266*, 282–294.
18. Yin, W.; Yates, M. Z. Effect of Interfacial Free Energy on the Formation of Polymer Microcapsules by Emulsification/Freeze-Drying. *Langmuir* **2008**, *24*, 701–708.
19. Han, J.; Song, G.; Guo, R. Synthesis of Polymer Hollow Spheres with Holes in Their Surfaces. *Chem. Mater.* **2007**, *19*, 973–975.
20. Im, S. H.; Jeong, U. Y.; Xia, Y. Polymer Hollow Particles with Controllable Holes in Their Surfaces. *Nat. Mater.* **2005**, *4*, 671–675.
21. Chen, J.; McLellan, J. M.; Siekkinen, A.; Xiong, Y.; Li, Z. Y.; Xia, Y. Facile Synthesis of Gold−Silver Nanocages with Controllable Pores on the Surface. *J. Am. Chem. Soc.* **2006**, *128*, 14776–14777.
22. Chen, T.; Yang, M.; Wang, X.; Tan, L. H.; Chen, H. Controlled Assembly of Eccentrically Encapsulated Gold Nanoparticles. *J. Am. Chem. Soc.* **2008**, *130*, 11858–11859.
23. Yang, M.; Chen, T.; Lau, W. S.; Wang, Y.; Tang, Q.; Yang, Y.; Chen, H. Development of Polymer-Encapsulated Metal Nanoparticles as Surface-Enhanced Raman Scattering Probes. *Small* **2008**, *5*, 198–202.
24. Nie, Z. H.; Fava, D.; Rubinstein, M.; Kumacheva, E. "Supramolecular" Assembly of Gold Nanorods End-Terminated with Polymer "Pom-Poms": Effect of Pom-Pom Structure on the Association Modes. *J. Am. Chem. Soc.* **2008**, *130*, 3683–3689.
25. Chen, H.; Abraham, S.; Mendenhall, J.; Delamarre, S. C.; Smith, K.; Kim, I.; Batt, C. A. Encapsulation of Single Small Gold Nanoparticles by Diblock Copolymers. *ChemPhysChem* **2008**, *9*, 388–392.
26. Kang, Y.; Taton, T. A. Core/Shell Gold Nanoparticles by Self-Assembly and Crosslinking of Micellar, Block-Copolymer Shells. *Angew. Chem., Int. Ed.* **2005**, *44*, 409–412.
27. Chen, G.; Wang, Y.; Tan, L. H.; Yang, M.; Tan, L. S.; Chen, Y.; Chen, H. High-Purity Separation of Gold Nanoparticle Dimers and Trimers. *J. Am. Chem. Soc.* **2009**, *131*, 4218–4219.
28. Tsagaropoulos, G.; Eisenberg, A. Direct Observation of Two Glass Transitions in Silica-Filled Polymers. Implications to the Morphology of Random Ionomers. *Macromolecules* **1995**, *28*, 396–398.
29. *Engineered Materials Handbook: Engineering Plastics*; ASM International, **1988**; Vol. 2.
30. Frens, G. Controlled Nucleation for the Regulation of the Particle Size in Monodisperse Gold Suspensions. *Nat. Phys. Sci.* **1973**, *241*, 20–22.
31. Nikoobakht, B.; El-Sayed, M. A. Preparation and Growth Mechanism of Gold Nanorods (NRs) Using Seed-Mediated Growth Method. *Chem. Mater.* **2003**, *15*, 1957–1962.
32. Jana, N. R.; Gearheart, L.; Murphy, C. J. Wet Chemical Synthesis of High Aspect Ratio Cylindrical Gold Nanorods. *J. Phys. Chem. B* **2001**, *105*, 4065–4067.
33. Skrabalak, S. E.; Au, L.; Li, X.; Xia, Y. Facile Synthesis of Ag Nanocubes and Au Nanocages. *Nat. Protocols* **2007**, *2*, 2182–2190.